Knockdown of Claudin-19 in the Retinal Pigment Epithelium Is Accompanied by Slowed Phagocytosis and Increased Expression of SQSTM1

Fanfei Liu,[1–3] Shaomin Peng,[1] Ron A. Adelman,[3] and Lawrence J. Rizzolo[2,3]

[1]Aier School of Ophthalmology, Central South University, Changsha, China
[2]Department of Surgery, Yale University, New Haven, Connecticut, United States
[3]Deparment of Ophthalmology and Visual Science, Yale University, New Haven, Connecticut, United States

Correspondence: Lawrence J. Rizzolo, Department of Surgery, Yale University, New Haven, CT 06520-8062, USA; lawrence.rizzolo@yale.edu.
Shaomin Peng, Aier School of Ophthalmology, Central South University, Floor 4, New Century Building, No. 198, Section 2, Furong Middle Road, Changsha 410015, China; pengshaomin@aierchina.com.

Received: August 18, 2020
Accepted: January 22, 2021
Published: February 16, 2021

Citation: Liu F, Peng S, Adelman RA, Rizzolo LJ. Knockdown of claudin-19 in the retinal pigment epithelium is accompanied by slowed phagocytosis and increased expression of SQSTM1. *Invest Ophthalmol Vis Sci.* 2021;62(2):14. https://doi.org/10.1167/iovs.62.2.14

Purpose. Besides regulating paracellular diffusion, claudin-19 modulates the expression of proteins essential for the retinal pigment epithelium (RPE). This study asks how RPE responds when the expression of claudin-19 is reduced.

Methods. In stem cell-derived RPE, claudin-19 and sequestosome-1/p62 (SQSTM1) were knocked down with siRNAs. Expression was monitored by quantitative RT-PCR and western blotting. Morphology and function were monitored by immunocytochemistry and transepithelial electrical resistance (TER). Phagocytosis of photoreceptor outer segments (POSs) was followed by fluorescence-activated cell sorting and western blotting. Pharmacology was used to assess the effects of AMP-activated protein kinase (AMPK) and SQSTM1 on phagocytosis. Enzymatic activity was measured using commercial assay kits.

Results. Knockdown of claudin-19 reduced the TER without affecting the integrity of the apical junctional complex, as assessed by the distribution of zonula occludens-1 and filamentous actin. AMPK was activated without apparent effect on autophagy. Activation of AMPK alone had little effect on phagocytosis. Without affecting ingestion, knockdown reduced the rate of POS degradation and increased the steady-state levels of LC3B and SQSTM1. Proteasome inhibitors also retarded degradation, as did knockdown of SQSTM1. The expression of metallothioneins and the activity of superoxide dismutase increased.

Conclusions. Knockdown of claudin-19 slowed the degradation of internalized POSs. The study questions the role of activated AMPK in phagocytosis and suggests a role for SQSTM1. Further, knockdown was associated with a partial oxidative stress response. The study opens new avenues of experimentation to explore these essential RPE functions.

Keywords: retinal pigment epithelium, claudin-19, SQSTM1, phagocytosis, AMPK, oxidative stress

The retinal pigment epithelium (RPE) is unique among epithelia. Instead of a lumen, its apical surface is closely juxtaposed to a solid tissue, the neurosensory retina. The apical microvilli of RPE interdigitate with the outer segments of the photoreceptors, and RPE phagocytizes the disc membranes shed by the photoreceptors.[1] Together with the choriocapillaris and intervening Bruch's membrane on its basal side, RPE forms the outer blood–retinal barrier.[2,3] Accordingly, RPE provides nutrients, regulates the environment of the subretinal space, absorbs water and stray light, participates in the visual cycle, and secretes factors essential for the health of the choriocapillaris and the neurosensory retina.

A distinctive feature of RPE is its enormous phagocytic capacity.[1] Photoreceptors shed disc membranes from the tips of their outer segments on a daily basis. RPE phagocytizes and degrades the photoreceptor outer segments (POSs) through a multistep process that includes ingestion, intracellular transport of the phagosome, maturation, and degradation. Dysfunctional phagocytosis is at the heart of many macular degenerative diseases.[4–9] Accumulation of undigested POSs leads to the formation of lipofuscin, a potent photoinducible generator of reactive oxygen species.[10] This effect adds to the oxidative stress that is normally present due to the high rate of oxygen consumption by the retina.[11] Besides mitochondria and light radiation, reactive oxygen species are generated by the process of phagocytosis itself.[12,13] To survive, mechanisms are essential for RPE to ameliorate the oxidative destruction of lipids, proteins, and organelles. Overwhelmed or diminished antioxidant mechanisms appear to be a significant component of age-related macular degeneration.[14]

The current study examines how tight junctions might affect phagocytosis and antioxidation mechanisms. Tight junctions are a continuous band that encircles the apical end of the lateral plasma membrane, binding cells to their neighbors and limiting transepithelial diffusion across the paracellular space. The junctions form a semipermeable, semiselective seal whose properties are determined by members of the claudin family of proteins. The claudin that lends RPE-

specific properties is claudin-19. In addition to the barrier function, a growing literature demonstrates that claudins are signaling proteins.[2,15] Directly, or indirectly, claudin-19 modulates the expression of a number of proteins essential for the functions of RPE.[16–18] We focused on three proteins affected by a knockdown of claudin-19.

A possible tie among tight junctions, autophagy, and phagocytosis is AMP-activated protein kinase (AMPK). AMPK is an energy sensor that regulates anabolic and catabolic pathways according to the energy needs of the cell.[19] Autophagy is a catabloic pathway that degrades and recycles damaged organelles and proteins. In addition to autophagy, AMPK also participates in the reassembly of dissociated tight junctions.[20–23] Studies with the adult retinal pigment epithelial (ARPE19) cell line indicate a role for AMPK in inhibiting phagocytosis.[24,25] Microtubule-associated protein 1 light chain 3B (LC3B) lies at the intersection of autophagy and a form of phagocytosis, LC3-associated phagocytosis (LAP).[26–30] Sequestosome-1/p62 (SQSTM1) is a bridge between autophagy and degradation by proteasomes. SQSTM1 is a receptor for ubiquitinated cargoes and delivers them to autophagosomes.[31,32] Further, SQSTM1 directs autophagosomes to lysosomes and ubiquinated proteins to proteasomes.[33,34] We investigated the interrelations of these proteins and suggest a link between SQSTM1 and phagocytosis.

Materials and Methods

Differentiation of RPE from Human-Induced Pluripotent Stem Cells

The human-induced pluripotent stem cell (hiPSC) line, IMR90-4, was obtained from WiCell Research Institute (Madison, WI, USA) and differentiated into RPE, as previously described.[35] RPE was cultured on 12-mm Transwell inserts (Costar 3460; Corning, Lowell, MA, USA) that were coated with Corning Synthemax (5 µg/filter). RPE cells maintained in knockout serum replacement-based media with 10-µM rock inhibitor until cells were fully confluent. Cultures were then switched to serum-free media (SFM) (DMEM/F12, high glucose, 3:1; 2% B-27 Supplement; 1-mM sodium pyruvate; 2-mM glutamax; 100-U/mL penicillin; 100 µg/mL streptomycin; Thermo Fisher Scientific, Waltham, MA, USA) for 60 to 90 days until the transepithelial electrical resistance (TER) reached a plateau. TER was measured with an epithelial voltohmmeter (EVOM) resistance meter using EndOhm electrodes (World Precision Instruments, Sarasota, FL, USA).[36]

Small Interfering RNA

The small interfering RNAs (siRNAs) for knockdown experiments were obtained from Dharmacon (Lafayette, CO, USA) The knockdowns were performed according to the manufacturer's protocol. Briefly, cultures of iPSC–RPE cells were fully differentiated and then were transfected using 25-nM siRNA (*CLDN19* or *CLDN4*) or 50-nM siRNA (*SQSTM1* and the controls *PPIB* [cyclophilin B]), and DharmaFECT 4 transfection reagent alone. The siRNA *CLDN4* served as a negative control, as claudin-4 is not expressed by iPSC–RPE, and *PPIB* was a control recommended by Dharmacon. Cells were incubated with siRNA for 48 hours, then returned to SFM. Experiments were performed at 1 week post-transfection.

Western Blotting

Total protein was isolated in ice-cold lysis buffer (0.1% SDS and 50-mM Tris, pH 8.0) with a protease inhibitor cocktail (Sigma Aldrich, Saint Louis, MO, USA). Protein concentrations were measured by nanodrop spectrophotometry. Following electrophoresis, the proteins were transferred to polyvinylidene fluoride membranes and incubated in blocking buffer for 2 hours at room temperature (RT) and then in primary antibody overnight at 4°C. Primary antibodies were detected by incubation with secondary antibodies conjugated with horseradish peroxidase. Antibodies are described in Supplementary Table S1. β-actin was used for the loading control.

Immunofluorescence and Confocal Microscopy

Cultures were fixed in 2% paraformaldehyde for 5 minutes at RT, permeabilized with 0.1% Triton X-100 (Bio-Rad Laboratories, Hercules, CA, USA) in PBS buffer, and blocked with 5% normal donkey serum (S30; EMD Millipore, Burlington, MA, USA) for 2 hours at RT. The cultures were incubated with primary antibodies (Supplementary Table S1) overnight at 4°C, followed by the appropriate secondary antibodies. Invitrogen Alexa Fluor 647 phalloidin (Thermo Fisher Scientific) was used to label F-actin. Then, 4′,6-diamidino-2-phenylindole (DAPI) was used to label the nucleus. Cultures were mounted with Fluoromount-G (SouthernBiotech, Birmingham, AL, USA).

Phagocytosis Assays

Porcine photoreceptor outer segments were isolated using the protocol established by Mao and Finnemann.[37] RPE was incubated with POSs in SFM for 2 hours at 37°C in a humidified CO_2 incubator. Cultures were washed with 0.5-mM EDTA in 1× PBS to remove bound and unbound POSs. In most experiments, cells were incubated for 6 more hours. In some experiments, cells were incubated for 0, 6, 24, 48, and 96 hours. Cell lysates were analyzed by western blotting. Samples were blotted with anti-rhodopsin antibodies, and the intensity of the bands was normalized to actin. Because rhodopsin forms multimers, all of the multimers were integrated when quantifying the blots.

Alternatively, phagocytosis was analyzed using a fluorescence-activated cell sorter (FACS). Bovine rod POSs, labeled with fluorescein isothiocyanate (FITC; Sigma-Aldrich) were fed to RPE cultured on Transwell filters (~25 POS particles/RPE cell). The cultures were incubated for 2 hours at 37°C in a humidified CO_2 incubator. Cultures were then rinsed with growth medium to remove excess FITC–POS, and the incubation continued for 3 more hours. The cells were harvested with 0.25% Trypsin–EDTA and washed with 1× PBS containing 2% fetal bovine serum. FACS data were analyzed with BD FACSDIVA software (BD Biosciences, San Jose, CA, USA).

Pharmacology Experiments

For all experiments, 500 µL of 100-µM bafilomycin A1, 100-nM marizomib, 75 mM 5-aminoimidazole-4-carboxamide riboside (AICAR), or 20-nM dorsomorphin in SFM was added to the apical medium chamber of the Transwell insert, incubated in a 37°C incubator for 24 hours, and assayed for phagocytosis. Western blotting for AMPK, phosphorylated

Investigative Ophthalmology & Visual Science

AMPK (pAMPK), and rhodopsin was performed following a 2-hour incubation with POSs and 6-hour incubation without POSs, as described above.

Quantitative Real-Time, Reverse-Transcriptase PCR

Total RNA was extracted using the RNeasy Mini Kit (Qiagen, Hilden, Germany). cDNA was reverse transcribed according to the manufacturer's instructions (iScript cDNA Synthesis Kit; Bio-Rad). PCR primers are listed in Supplementary Table S2. Experiments were performed in three biological repeats. *GAPDH* was used as a control to normalize the data. Relative mRNA expression was calculated using the $2^{-\Delta\Delta Ct}$ method.[38]

Enzyme Assays

Catalase and superoxide dismutase (SOD) assay kits were purchased from Cayman Chemical (Ann Arbor, MI, USA). Cells were scraped from the Transwell filter in PBS and centrifuged. Cell lysates were centrifuged at 1500*g* for 5 minutes at 4°C. Supernatants (10 uL) were assayed according to the manufacturer's instructions. Three independent experiments were performed.

Statistics

Statistical analyses performed using Prism 8 (GraphPad Software, San Diego, CA, USA) included Student's *t*-test for two-way comparisons, Student's one-way *t*-test to compare the deviation of ratios from 1.0, and Pearson's correlation coefficient. The number of independent experiments is indicated in the figure legends. $P < 0.05$ was considered significant.

Results

Effects of Knocking Down Claudin-19 on the Apical Junctional Complex and a Potential Role for pAMPK

RPE was differentiated from hiPSCs, and *CLDN19* was knocked down using siRNA. As controls, RPE was mock transfected or transfected with siRNAs to *PPIB* (cyclophilin B) and *CLDN4*, a claudin not expressed by RPE.[39] Consistent with our earlier studies,[17,18,39] the siRNA directed against *CLDN19* reduced the expression of claudin-19 and reduced the TER (Fig. 1). The decreases in TER and expression of claudin-19 required a week after the second treatment with siRNA, suggesting a long half-life for claudin-19 as reported for claudin-2.[40] The TER began to increase after 3 weeks, demonstrating the viability of the cultures. The slow recovery is consistent with a variety of RPE culture models, including hiPSC–RPE. After replating RPE, adherens junctions reassemble quickly, but reassembly of tight junctions requires 4 to 6 weeks.[41] Accordingly, TER was used to assess the effectiveness of the knockdown. For cultures that were effectively knocked down, the 1-week time point was used to initiate analysis of each siRNA experiment. Figure 1B confirmed that the expression of claudin-19 was low for the duration of the experiments described below. Despite the decreased expression of claudin-19, zonula occludens-1 (ZO-1) and filamentous actin remained in circumferential bands in the position of the apical junctional complex (Fig. 2).

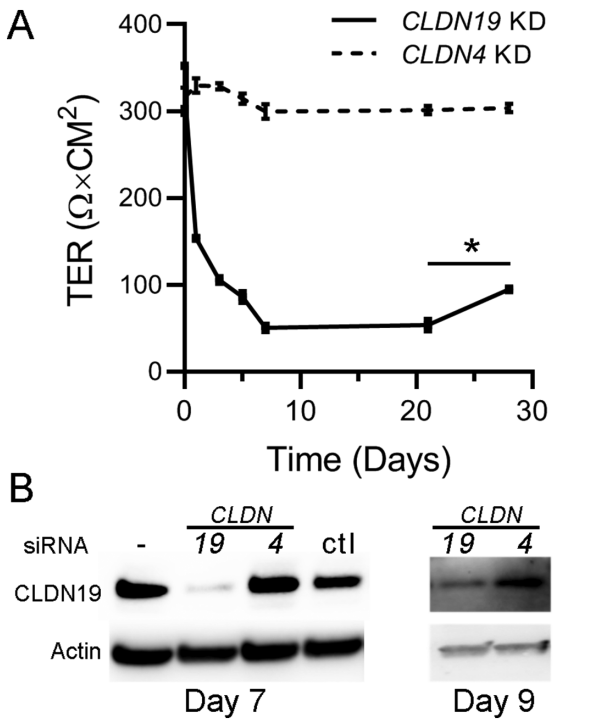

Figure 1. Knockdown of *CLDN19* greatly reduced the expression of claudin-19. hiPSC–RPE was transfected two times with siRNA to *CLDN19*, *CLDN4*, or a control RNA (*PPIB,* ctl), as described in the Supplementary Materials. (**A**) TER was measured before transfection. One week after the second transfection, TER reached is minimal value. After 3 weeks, the TER began to recover. Time "0" is one day before the start of the experiment; Time "10" is 10 days after the second transfection; *error bars* (SE) are shown in place of symbols ($n = 6$). (**B**) After day 7 and day 9, protein extracts were immunoblotted. Only the siRNA to *CLDN19* reduced the expression of claudin-19. The expression of claudin-19 remained low when some of the following experiments were performed 8 or 9 days after the second transfection. *$P < 0.005$ ($n = 3$).

These data indicated that tight junctions were disrupted, but the adherens junction portion of the apical junctional complex remained intact. When the apical junctional complex is completely disassociated, reassociation of the complex requires activation (phosphorylation) of AMPK.[20–23] AMPK is an energy sensor that can activate, or inactivate, anabolic and catabolic pathways depending on the AMP/ATP ratio,[23,42,43] but its effects on the reassembly of tight junctions are independent of energy levels. In the current study, reducing the amount of claudin-19 alone was sufficient to increase the pAMPK/AMPK ratio relative to the *CLDN4* KD control (Fig. 3). Activated AMPK can inhibit anabolic pathways and stimulate catabolic pathways, including autophagy. In the knockdown experiments, pAMPK had little effect on Unc-51-like kinase 1 (ULK1), an upstream kinase in the autophagy pathway, and phosphorylation decreased for Raptor-1, an indirect activator of ULK1.[44,45]

Effects of Claudin-19 Knockdown on Phagocytosis and a Role for SQSTM1

In ARPE19 cells, pAMPK inhibited phagocytosis.[24,25] Knockdown of claudin-19 did reduce the rate of phagocytosis (Figs. 4A, 4B). hiPSC–RPE was transfected with an siRNA

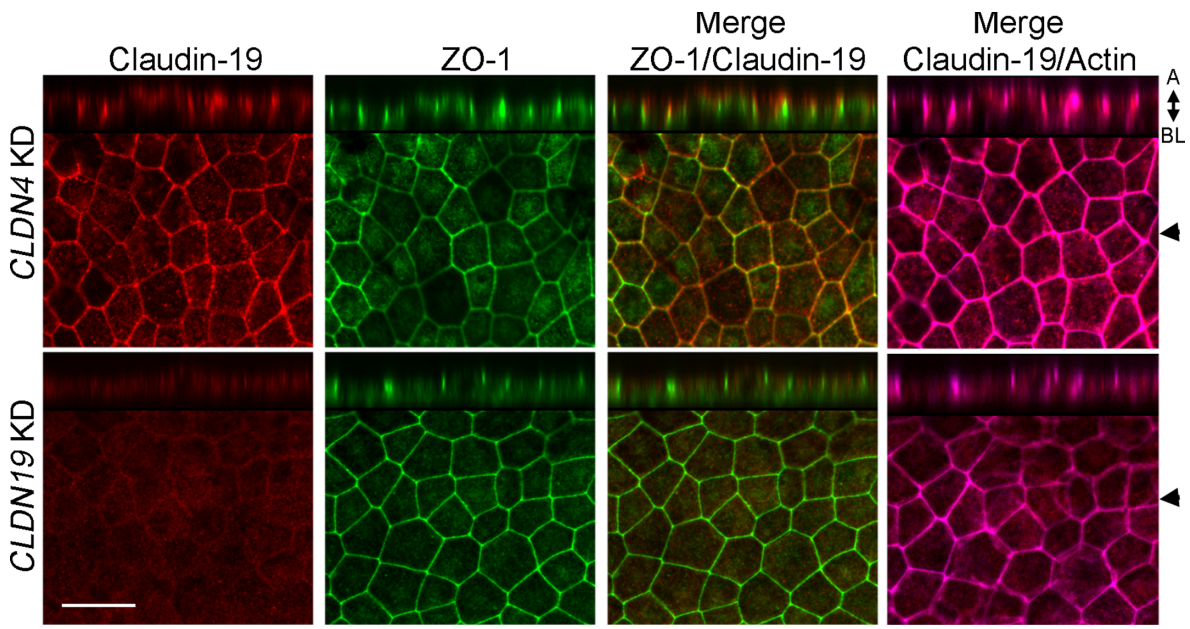

Figure 2. Knockdown of *CLDN19* did not disrupt the apical junctional complex. One-week after transfection, when the TER for the *CLDN19* knockdown was ~50 Ω × cm^2, cultures were labeled with antibodies to claudin-19 (*red*) or ZO-1 (*green*) and counterstained with phalloidin to reveal filamentous actin (*magenta*). Cultures were imaged by confocal microscopy. Claudin-19 co-localized with ZO-1 and actin in the *CLDN4* KD control. When the expression of claudin-19 was suppressed, ZO-1 and actin remained in circumferential bands indicative of an intact apical junctional complex. Images representative of three experiments. *Arrowheads* indicate locations on the *x,y* plane for the corresponding *xz* plane; *double-headed arrow* indicates the apical (A) and basal (BL) membranes in the *xz* plane, *Scale bar*: 20 µm.

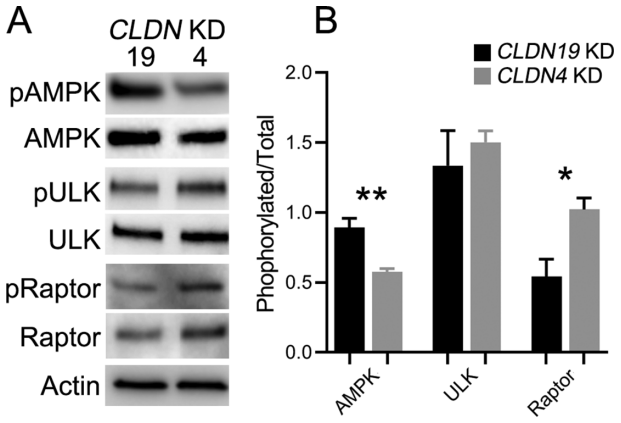

Figure 3. Knockdown of *CLDN19* increased the phosphorylation of AMPK but not downstream kinases along the autophagy pathway. (**A**) Cultures were treated with siRNAs directed against *CLDN19* or *CLDN4*, and western blots were prepared 1 week after the second transfection. (**B**) The ratio of phosphorylated kinase to total kinase was plotted. *Error bars* denote SE ($n = 3$); $^{*}P < 0.05$, $^{**}P < 0.01$.

to *CLDN19* or *CLDN4*. On day 7 after the second transfection, POSs were fed to the RPE for 2 hours followed by an EDTA wash to remove surface-bound and unbound POSs. The culture was continued in the absence of POSs, and RPE was harvested at various times up to 96 hours. (Note that 48 hours corresponds to day 9 in Fig. 1.) Protein extracts were prepared and immunoblotted for rhodopsin. The intensity of the rhodopsin signal was quantified by normalizing its intensity to actin. The degradation of rhodopsin was retarded by the claudin-19 knockdown relative to the claudin-4 knockdown (Fig. 4). Binding and ingestion of POSs were unaffected by the knockdown, as indicated by FACS analysis. RPE was incubated with FITC-labeled POSs for 2 hours, the POSs were removed, and the culture continued for 3 more hours. Single cells were harvested by trypsinization, and the percentage of FITC-labeled cells was determined (Fig. 4C, Supplementary Fig. S1). Approximately 23% of cells ingested POSs. No statistical difference was found among the mock control, claudin-19 knockdown, and claudin-4 knockdown. Rather than an effect on binding or internalization, these data support an effect on intracellular transport of the phagosome, maturation, or degradation.

Unlike the ARPE19 study noted above, we could not link pAMPK to phagocytosis. The ARPE19 study used 5-amino-imidazole-4-carboxamide-1-β-D-ribofuranoside (AICAR), an AMP mimetic, to activate AMPK. The result was that MerTK was inactivated, thereby inhibiting the internalization of POSs.[24,25] We could not replicate that result in hiPSC–RPE (Fig. 5). In claudin-19 knockdown experiments, inhibiting AMPK with dorsomorphin failed to block the effect of the knockdown. If anything, dorsomorphin appeared to slightly retard the degradation of POSs even in the claudin-4 control. As a check on viability, the experimental procedures did not affect the TER of cultures knocked down with siRNA to either *CLDN19* or *CLDN4* (Supplementary Fig. S2).

Further examination of phagocytosis and autophagy revealed effects on the expression of LC3B and SQSTM1 (Fig. 6). Quantitative real-time, reverse-transcriptase PCR (qRT^2-PCR) was used to compare the expression of relevant mRNAs in the claudin-19 knockdown relative to that of claudin-4. The only effect was to increase the expression of SQSTM1 by ~14 times ($P < 0.01$). SQSTM1 is an adapter protein that, in conjunction with LC3B, sequesters specific, ubiquitinated cargoes into autophagosomes.[46] Western blotting

Investigative Ophthalmology & Visual Science

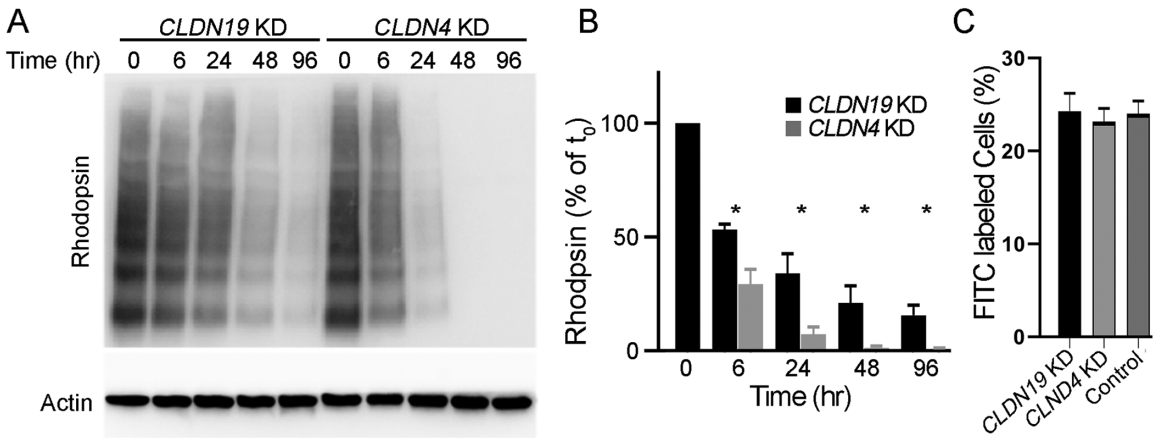

Figure 4. Knockdown of *CLDN19* slowed the degradation of phagocytized POSs. Cultures were transfected with siRNA. One week after the second transfection, cultures were incubated with POSs for 2 hours followed by an EDTA wash to remove non-phagocytized POSs. Cultures were continued for up to 96 hours. (**A**) At the indicated times, protein extracts were analyzed by western blotting. Rhodopsin and all its multimers were evident on the blots. With knockdown of *CLDN4*, rhodopsin was completely degraded by 48 hours. In the *CLDN19* knockdown cultures, rhodopsin was still evident at 96 hours. (**B**) Blots were quantified by normalizing the rhodopsin signal to actin. (**C**) Cultures were transfected or mock transfected (control) and incubated with POSs, as above. POSs were removed, the incubation continued for 3 hours, and cells were harvested for FACS analysis (Supplementary Fig. S1). *Error bars* indicate SE (B, $n = 4$; C, $n = 3$); $^{*}P < 0.05$.

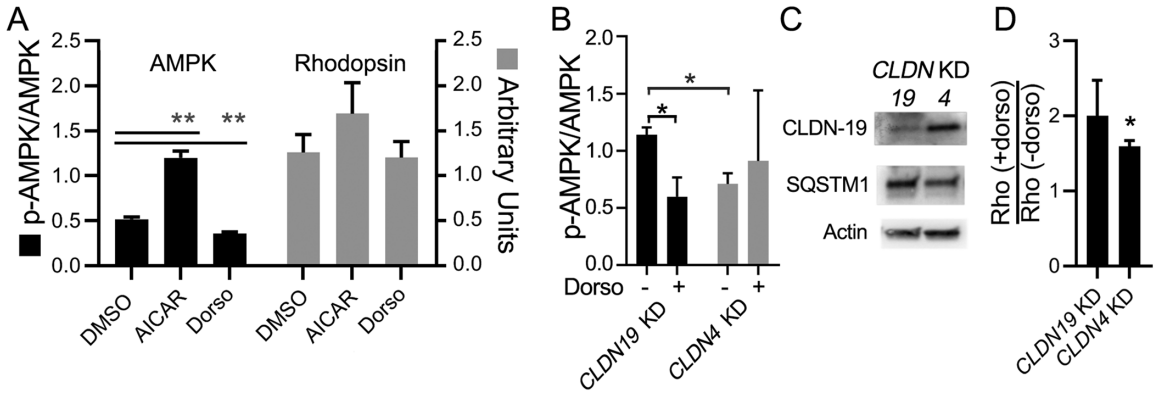

Figure 5. Phosphorylation of AMPK with and without *CLDN19* knockdown failed to affect phagocytosis and degradation of POSs. (**A**) Phosphorylation of AMPK was stimulated by AICAR or inhibited by dorsomorphin (*black bars*). Cultures were treated with AICAR or dorsomorphin (Dorso) for 24 hours. Cultures were then incubated with POSs for 2 hours followed by an EDTA wash to remove non-phagocytized POSs. Six hours later, protein extracts were isolated for western blotting. As expected, AICAR phosphorylated AMPK and dorsomorphin dephosphorylated it. Neither AICAR nor dorsomorphin had any effect on the phagocytosis of POSs (*gray bars*). *Error bars* indicate SE ($n = 4$); $^{**}P < 0.002$. (**B–D**) Cultures were knocked down with either *CLDN19* or *CLDN4* before being treated with dorsomorphin 7 days after the second transfection. Degradation of POSs was assayed, as in **A**, and the ratio of degradation with or without dorsomorphin was determined (n = 3). (**B**) Dorsomorphin blocked the phosphorylation of AMPK that resulted from *CLDN19* KD. (**C**) Nine days after the second transfection, the expression of claudin-19 remained low relative to the *CLDN4* KD, and the expression of SQSTM1 was elevated. (**D**) Dorsomorphin failed to prevent *CLDN19* KD from retarding the degradation of POSs, as would be indicated by a ratio < 1.0. If anything, dorsomorphin further inhibited degradation. A small, but statistically significant, deviation from 1.0 was observed for the *CLDN4* KD. *Error bars* indicate SE ($n = 3$); $^{*}P < 0.05$.

revealed that suppressed expression of claudin-19 increased steady-state levels of SQSTM1 by 112% ($P < 0.01$). The steady-state level of LC3B increased by ~79% ($P < 0.01$). No effect of claudin-19 knockdown was observed for ATG5, beclin-1, or PI3KC3. Although slight, there was a statistically significant increase in ubiquitinated proteins ($P < 0.05$). Because SQSTM1 targets some of its ubiquitinated cargoes to autophagosomes and others to proteasomes, regulation of its steady-state levels is complex.[29,33,34] We are unaware of reports that link SQSTM1 to phagocytosis. To explore a possible connection of SQSTM1 with phagocytosis, we first manipulated degradation by proteasomes.

Marizomib is a specific inhibitor of the proteasomal degradation of cytosolic proteins.[47] As expected, inhibition increased the steady-state levels of SQSTM1 but not LC3. In this circumstance, SQSTM1 is sequestered into large aggregates of ubiquitinated proteins.[48] Inhibition of proteasomes also retarded the degradation of phagocytized rhodopsin as well as, or better than, inhibition of lysosomes (Fig. 7A, Supplementary Fig. S3). Because rhodopsin is not degraded by proteasomes, a plausible explanation for the effect of marizomib was that SQSTM1 was sequestered into an inactive pool and unavailable for phagocytosis.

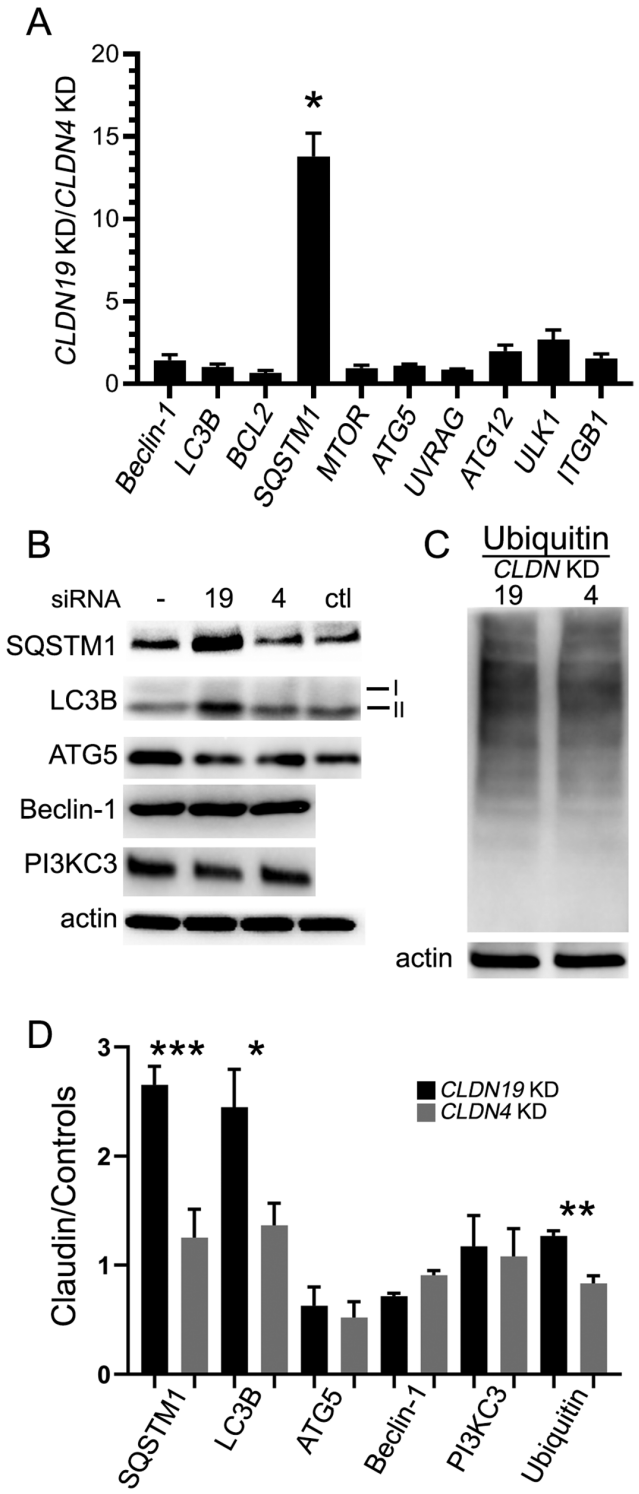

Figure 6. Knockdown of *CLDN19* increased the expression of SQSTM1 and LC3B but not other autophagy related proteins. One week after the second transfection, cultures were mock transfected (–) or transfected with an siRNA directed against *CLDN19* or *CLDN4* or with a commercial control siRNA (*PPIB*, ctl). Cells were harvested 1 week later. (**A**) mRNA was isolated and analyzed by qRT^2-PCR. Data, normalized to Glyceraldehyde 3-phosphate dehydrogenase (GAPDH), was plotted as the ratio of expression in the *CLDN19* and *CLDN4* knockdowns. Only the mRNA for *SQSTM1* was affected. *Error bars* indicate SE ($n = 3$); $^*P < 0.001$. (**B**, **C**) Cell lysates were resolved by sodium dodecyl sulfate (SDS)–gel electrophoresis and immunoblotted with the antibodies indicated in the figures. (**B**) Bars to the right indicate the positions of LC3B-I and LC3B-II. A representative blot is included for the loading control, actin. (**C**) Blots were probed with anti-ubiquitin antibodies to reveal total ubiquitinated proteins. (**D**) The western blots were quantified by normalizing the blots to actin. The data are plotted as the ratios of claudin intensity to the average intensity of the controls (mock and siRNA$_{PPIB}$-transfected samples). *Error bars* indicate SE ($n = 13$ for SQSTM1 and LC3; $n = 3$ for ATG5, Beclin-1, PI3KC3, and ubiquitin); $^*P < 0.02$, $^{**}P < 0.005$, $^{***}P < 0.002$.

To test the hypothesis that SQSTM1 participates in phagocytosis, *SQSTM1* was knocked down with an siRNA followed by an incubation with POSs for 2 hours (Fig. 7B). After washing with EDTA, cultures were continued for 6 hours, the cells were harvested, and the amount of rhodopsin remaining in the cells was quantified by western blotting. The knockdown of SQSTM1 was variable. Accordingly, the amount of rhodopsin was normalized to the negative control, siRNA for cyclophilin B, and plotted as a function of the percentage of SQSTM1 that was knocked down. The amount of undigested rhodopsin linearly correlated with the percentage of SQSTM1 that was knocked down (Pearson correlation coefficient = 0.904).

Effects of Claudin-19 Knockdown on Elements of an Antioxidation Response

Reports that increased SQSTM1 is associated with an oxidation response prompted us to examine whether the knockdown of claudin-19 engendered such a response.[49] Two enzymes that neutralize reactive oxygen species are catalase and SOD. Enzymatic activity for catalase was not detected, but SOD was evident in hiPSC–RPE (Fig. 8). The claudin-19 knockdown resulted in a twofold increase in SOD activity relative to activity in *CLDN4* knockdowns ($P < 0.003$). Catalase activity remained undetected. Another protection against oxidative stress, including the stress induced by phagocytosis, is provided by metallothioneins.[12,50] qRT^2-PCR revealed that the expression of at least five family members increased two to three times ($P < 0.05$) (Fig. 8). A third mechanism to relieve oxidative stress is tyrosinase, a key enzyme for the biosynthesis of melanin granules. Although melanin granules are not formed in adults, tyrosinase can be upregulated by oxidative stress and is more effective than melanin granules in relieving it.[51–53] Further, exogenous expression of claudin-19 in ARPE19 decreased the steady-state level of tyrosinase.[16] Nonetheless, an increase in the steady-state levels of tyrosinase was not observed in the current study by western blotting.

Discussion

Tight junctions are signaling complexes that transmit signals into the cell to regulate gene transcription, cell morphology, and cell proliferation (for reviews, see References 2, 15, and 54). In a variety of human and mouse models of RPE, we have shown that claudin-19 affects the expression of proteins for essential RPE functions.[17,18] Nonetheless, the effects reported here for the knockdown of claudin-19 might be related to a general stress response induced by impairing the structure or function of tight junctions. Four lines of evidence combined to suggest a stress response: activation of AMPK, increased expression of SQSTM1, slowed degradation of POSs, and increased expression or activity of antioxidants.

Investigative Ophthalmology & Visual Science

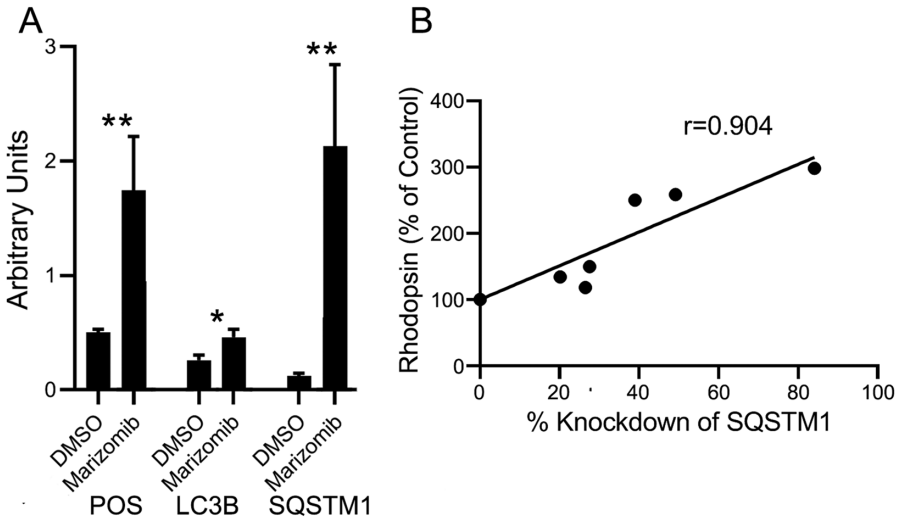

Figure 7. Reduced availability of SQSTM1 retarded the degradation of rhodopsin. (**A**) To sequester SQSTM1 into protein aggregates, proteasomes were inhibited with marizomib. Cultures were incubated for 24 hours in dimethylsulfoxide (DMSO) or DMSO plus marizomib. POSs were added for 2 hours, and the cultures were washed with EDTA to remove bound and unbound POSs and incubated for 6 more hours. Cell lysates were western blotted, and the intensity of the signals was normalized to the signal for actin. Marizomib retarded degradation of POSs and increased the steady-state levels of LC3B and SQSTM1. *Error bars* indicate SE ($n = 4$–9); $^{*}P < 0.05$; $^{**}P < 0.01$. (**B**) Cultures were transfected with an siRNA directed against *SQSTM1* or *PPIB* and incubated with POSs, as described in **A**. The signal for SQSTM1 and rhodopsin was normalized to the *PPIB* control. Because the efficiency of the knockdown was variable, data were plotted as a function of the percentage of SQSTM1 that was knocked down. The linear regression plot was forced through 100% of control, and the Pearson correlation coefficient was 0.904 ($n = 6$).

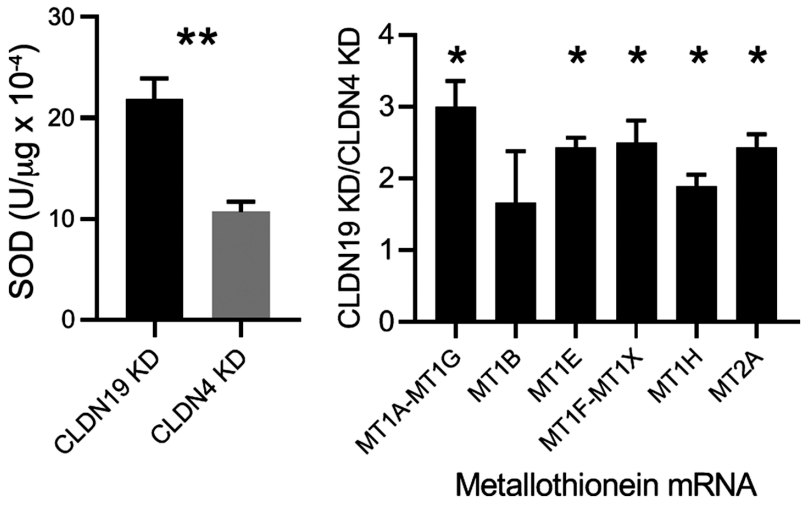

Figure 8. Knockdown of *CLDN19* resulted in increased activity of SOD and expression of metallothioneins. Cultures were harvested 1 week after transfection. (**A**) Cell lysates were assayed for SOD activity. (**B**) mRNA was isolated and prepared for qRT^2-PCR. Expression was normalized to GAPDH and then individual genes were normalized to expression of that gene in the *CLDN4* knockdown cultures. Statistical deviation from 1.0 was estimated by a one-way Student's *t*-test. The primers did not distinguish between *MT1A* and *MT1G* or between *MT1F* and *MT1X*. *Error bars* indicate SE ($n = 3$ for SOD; $n = 4$ for metallothionein); $^{*}P < 0.05$; $^{**}P < 0.003$.

AMPK

AMPK is a multifunctional protein that responds to environmental stressors and energy stress by inhibiting anabolic pathways, activating catabolic pathways, and mitigating oxidative stress.[23,42,43] AMPK also participates in the assembly and stabilization of the apical junctional complex without inducing autophagy.[20–23] pAMPK phosphorylates proteins of the adherens and tight junctions, including claudins. Reassembly of the apical junctional complex has been studied by completely disassociating the tight and adherens junctions of the complex and examining the reassembly of the complex. Phosphorylation of AMPK was essential for reassembly to occur. Confirming earlier studies with human fetal RPE,[39] we disrupted tight junctions, leaving the rest of the apical junctional complex intact. Removal of the dominant claudin in RPE was sufficient to activate AMPK.

We asked if there was a connection between activated AMPK and the effects of decreased claudin-19 on phagocytosis. In ARPE19, pAMPK inhibited phagocytosis by inactivating MerTK, a component of the mechanism for ingesting POSs.[24,25] We did not observe this phenomenon in hiPSC–RPE. Activation of AMPK with AICAR, or inhibition with dorsomorphin (which inhibits AMPK and other protein kinases[55]) had no effect on the degradation of rhodopsin. Dorsomorphin failed to block the effect of claudin-19 knockdown on phagocytosis. Further, knockdown of claudin-19 inhibited only the post-ingestion steps of the phagocytic pathway. Although ARPE19 manifests many aspects of native RPE, it may be a better model of diseased or aged RPE.[56] Further, the ARPE19 studies did not use growth conditions that differentiate the cell line. Accordingly, functional tight junctions likely failed to form.[57–59] Among its deficits, ARPE19 does not express claudin-19, and many RPE properties were restored when exogenous claudin-19 was expressed.[17] Using human fetal RPE as a gold standard, stem cell-derived RPE more closely resembles native RPE.[41,60–62]

The activation of AMPK described here might result from a feedback loop poised to reassemble the tight junction when claudin-19 reappeared. The stress response engendered by knocking down claudin-19 may be a separate effect. Autophagy is often activated by pAMPK and cellular stress, but we failed to find evidence of activated autophagy kinases or upregulation of autophagy genes. Further, increased flux through the autophagic pathway should decrease the steady-state levels of SQSTM1 and LC3B.[29] Instead, knockdown of claudin-19 increased the expression of both.

SQSTM1 and LC3-Associated-Phagocytosis

LAP co-exists in RPE with canonical phagocytosis.[26,28] Although an increase in LC3B would be expected if the degradation of phagosomes was impaired, we are unaware of reports that implicate SQSTM1 in LAP. With ubiquitin and LC3-binding domains, SQSTM1 is an adaptor protein that targets select ubiquitinated cargoes to either autophagosomes or to proteasomes. Whereas LC3B is associated with many pathways, there is a growing collection of adaptor proteins that alone, or in combination, bind LC3 to target specific organelles to lysosomes.[30] A new candidate for this group is melanoregulin, which is specific for phagosomes.[28] Notably, only a fraction of POS phagosomes are degraded via LAP.[1] Conceivably, a fraction of POS phagosomes are ubiquitinated. In this scenario, we propose that the ubiquitinated POS phagosomes might bind a complex that included melanoregulin, SQSTM1, and LC3B. Slowed degradation of this subset of phagosomes would lead to decreased degradation of LC3B and SQSTM1. This is consistent with the observation that most of the LC3B had been converted from the cytosolic form, LC3B-I, to the membrane-bound form, LC3B-II.

SQSTM1 bridges lysosomal and proteasomal catabolic pathways and is subject to numerous regulatory mechanisms.[29,33,34] Consequently, perturbation of one pathway might affect another. In the current study, inhibition of proteasomes affected degradation of POSs by the lysosomal pathway. We confirmed earlier reports that inhibition of proteasomes increased the steady-state level of SQSTM1. Those studies demonstrated that SQSTM1 was sequestered into large, undegraded protein aggregates along with its cargo of proteins damaged by oxidative and other stressors.[48,63] If inhibition of proteasomes sequestered SQSTM1 into a pool that was unavailable for LAP, then degradation of a subset of POSs might be inhibited. To test this hypothesis, we reduced the pool of available SQSTM1 with an siRNA knockdown. Reduced expression of SQSTM1 retarded the degradation of POSs (Fig. 7).

Increased expression of SQSTM1 and pAMPK is associated with several mechanisms that protect cells from oxidative and other stressors.[33,44] Knockdown of claudin-19 affected several mechanisms. Slowed degradation of POSs would reduce oxidative stress, because a burst of reactive oxygen species accompanies the fusion of phagosomes with lysosomes.[12,13] Mechanisms that ameliorate oxidative stress include metallothioneins and SOD. Knockdown of claudin-19 resulted in a two- to three-times increase in the expression of metallothionein family members. Knockdown also resulted in a two-times increase in activity for SOD.

Limitations

AMPK and SQSTM1 each lie at the nexus of multiple pathways related to stress. A shortcoming of this study is that the complexity of these pathways limited the depth at which they were studied. The few proteins we did study focus attention on parts of this regulatory network and point to directions for future research. The suggestion that SQSTM1 contributes to LAP should be studied in greater depth. Complete time courses are required to relate the effects on AMPK, LC3B, SQSTM1, and antioxidants to the time courses reported for claudin-19 knockdown and phagocytosis. Because phosphorylation events are often transient, similar time courses are needed to verify whether or not activation of AMPK lacked an effect on ULK1 and Raptor-1 (Fig. 3). Because of the prolonged protocol required to knockdown claudin, time courses should extend from when claudin-19 expression begins to decrease until expression recovers. Correlation of the time courses for claudin-19 and AMPK would help test the hypothesis that AMPK was activated as part of a feedback loop to reassemble tight junctions.

Tight junctions are essential elements of any epithelium. Impaired function might be expected to induce a stress response. Because of their central role in many stress-related pathways, it is not surprising that pAMPK and SQSTM1 would be among the responses. The observation that knockdown of SQSTM1 retarded the degradation of POSs suggests an intriguing possibility that SQSTM1 has a role in LAP. Further study is needed to explore the relationships among AMPK, LAP, and SQSTM1 to phagocytosis and the amelioration of oxidative stress. The observation that increased levels of SQSTM1/p62 are found in the macula of patients with age-related macular degeneration underscores the importance of such investigations.[64]

Acknowledgments

The authors thank Jie Gong, MD (Yale University) for providing the FITC-labeled POSs and her guidance in performing the FACS phagocytosis assay, and Hui Cai, PhD (Yale University) for help with some of the western blotting experiments.

Supported by grants from the National Natural Science Foundation of China (81570867, SP); Leir Foundation (RAA); Alonzo Family Fund (LJR); China Scholarship Council (201806370176, FL); Aier Eye Hospital Group Institute, Changsha, China (LJR);

Newman's Own Foundation (RAA); Science Research Foundation of Aier Eye Hospital Group (AF151D06, SP); Medical Technology Innovation Project, Hunan, China (2018SK50101, SP); Fundamental Research Funds for the Central Universities for the Central Universities of Central South University, Changsha, China (202221903, FL); Hunan Provincial Innovation Foundation for Postgraduate, Hunan, China (FL); and Research to Prevent Blindness (Yale University).

Disclosure: **F. Liu,** None; **S. Peng,** None; **R.A. Adelman,** None; **L.J. Rizzolo,** None

References

1. Lakkaraju A, Umapathy A, Tan LX, et al. The cell biology of the retinal pigment epithelium [published online ahead of print February 24, 2020]. *Prog Retin Eye Res*, https://doi.org/10.1016/j.preteyeres.2020.100846.
2. Fields MA, Del Priore LV, Adelman RA, Rizzolo LJ. Interactions of the choroid, Bruch's membrane, retinal pigment epithelium, and neurosensory retina collaborate to form the outer blood-retinal-barrier. *Prog Retin Eye Res*. 2020;76:100803.
3. Strauss O. The retinal pigment epithelium in visual function. *Physiol Rev*. 2005;85(3):845–881.
4. Sparrow JR, Boulton M. RPE lipofuscin and its role in retinal pathobiology. *Exp Eye Res*. 2005;80(5):595–606.
5. Singh R, Shen W, Kuai D, et al. iPS cell modeling of Best disease: insights into the pathophysiology of an inherited macular degeneration. *Hum Mol Genet*. 2013;22(3):593–607.
6. Singh R, Kuai D, Guziewicz KE, et al. Pharmacological modulation of photoreceptor outer segment degradation in a human iPS cell model of inherited macular degeneration. *Mol Ther*. 2015;23(11):1700–1711.
7. Marmorstein AD, Johnson AA, Bachman LA, et al. Mutant Best1 expression and impaired phagocytosis in an iPSC model of autosomal recessive bestrophinopathy. *Sci Rep*. 2018;8(1):4487–4487.
8. Keeling E, Lotery AJ, Tumbarello DA, Ratnayaka JA. Impaired cargo clearance in the retinal pigment epithelium (RPE) Underlies irreversible blinding diseases. *Cells*. 2018;7(2):16.
9. Esteve-Rudd J, Hazim RA, Diemer T, et al. Defective phagosome motility and degradation in cell nonautonomous RPE pathogenesis of a dominant macular degeneration. *Proc Natl Acad Sci USA*. 2018;115(21):5468–5473.
10. Boulton M, Rózanowska M, Rózanowski B, Wess T. The photoreactivity of ocular lipofuscin. *Photochem Photobiol Sci*. 2004;3(8):759–764.
11. Yu D-Y, Cringle SJ. Retinal degeneration and local oxygen metabolism. *Exp Eye Res*. 2005;80(6):745–751.
12. Tate DJ, Jr, Miceli MV, Newsome DA. Phagocytosis and H_2O_2 induce catalase and metallothionein gene expression in human retinal pigment epithelial cells. *Invest Ophthalmol Vis Sci*. 1995;36(7):1271–1279.
13. Miceli MV, Liles MR, Newsome DA. Evaluation of oxidative processes in human pigment epithelial cells associated with retinal outer segment phagocytosis. *Exp Cell Res*. 1994;214(1):242–249.
14. Beatty S, Koh H, Phil M, Henson D, Boulton M. The role of oxidative stress in the pathogenesis of age-related macular degeneration. *Surv Ophthalmol*. 2000;45(2):115–134.
15. González-Mariscal L, Domínguez-Calderón A, Raya-Sandino A, Ortega-Olvera JM, Vargas-Sierra O, Martínez-Revollar G. Tight junctions and the regulation of gene expression. *Semin Cell Dev Biol*. 2014;36:213–223.
16. Liu F, Xu T, Peng S, Adelman RA, Rizzolo LJ. Claudins regulate gene and protein expression of the retinal pigment epithelium independent of their association with tight junctions. *Exp Eye Res*. 2020;198:108157.
17. Peng S, Wang S-B, Singh D, et al. Claudin-3 and claudin-19 partially restore native phenotype to ARPE-19 cells via effects on tight junctions and gene expression. *Exp Eye Res*. 2016;151:1791–1789.
18. Wang S-B, Xu T, Peng S, et al. Disease-associated mutations of claudin-19 disrupt retinal neurogenesis and visual function. *Commun Biol*. 2019;2:113.
19. Mihaylova MM, Shaw RJ. The AMPK signalling pathway coordinates cell growth, autophagy and metabolism. *Nat Cell Biol*. 2011;13(2):1016–1023.
20. Rowart P, Wu J, Caplan MJ, Jouret F. Implications of AMPK in the formation of epithelial tight junctions. *Int J Mol Sci*. 2018;19(7):2040.
21. Zhang L, Li J, Young LH, Caplan MJ. AMP-activated protein kinase regulates the assembly of epithelial tight junctions. *Proc Natl Acad Sci USA*. 2006;103(46):17272–17277.
22. Zheng B, Cantley LC. Regulation of epithelial tight junction assembly and disassembly by AMP-activated protein kinase. *Proc Natl Acad Sci USA*. 2007;104(3):819–822.
23. Zhu M-J, Sun X, Du M. AMPK in regulation of apical junctions and barrier function of intestinal epithelium. *Tissue Barriers*. 2018;6(2):1–13.
24. Qin S. Blockade of MerTK activation by AMPK inhibits RPE cell phagocytosis. In: Bowes Rickman C, LaVail MM, Anderson RE, Grimm C, Hollyfield J, Ash J , eds. *Retinal Degenerative Diseases*. Cham: Springer International Publishing; 2016:773–778.
25. Qin S, Rodrigues GA. Roles of $\alpha v\beta 5$, FAK and MerTK in oxidative stress inhibition of RPE cell phagocytosis. *Exp Eye Res*. 2012;94(1):63–70.
26. Kim J-Y, Zhao H, Martinez J, et al. Noncanonical autophagy promotes the visual cycle. *Cell*. 2013;154(2):365–376.
27. Martinez J, Malireddi RKS, Lu Q, et al. Molecular characterization of LC3-associated phagocytosis reveals distinct roles for Rubicon, NOX2 and autophagy proteins. *Nat Cell Biol*. 2015;17(7):893–906.
28. Frost LS, Lopes VS, Bragin A, et al. The contribution of melanoregulin to microtubule-associated protein 1 light chain 3 (LC3) associated phagocytosis in retinal pigment epithelium. *Mol Neurobiol*. 2015;52(3):1135–1151.
29. Klionsky DJ, Abdelmohsen K, Abe A, et al. Guidelines for the use and interpretation of assays for monitoring autophagy (3rd edition). *Autophagy*. 2016;12(1):1–222.
30. Dhingra A, Bell BA, Peachey NS, et al. Microtubule-associated protein 1 light chain 3B (LC3B) is necessary to maintain lipid-mediated homeostasis in the retinal pigment epithelium. *Front Cell Neurosci*. 2018;12:351.
31. Johansen T, Lamark T. Selective autophagy mediated by autophagic adapter proteins. *Autophagy*. 2011;7(3):279–296.
32. Weidberg H, Shvets E, Elazar Z. Biogenesis and cargo selectivity of autophagosomes. *Annu Rev Biochem*. 2011;80:125–156.
33. Liu WJ, Ye L, Huang WF, et al. p62 links the autophagy pathway and the ubiqutin-proteasome system upon ubiquitinated protein degradation. *Cell Mol Biol Lett*. 2016;21:29.
34. Nam T, Han JH, Devkota S, Lee H-W. Emerging paradigm of crosstalk between autophagy and the ubiquitin-proteasome system. *Mol Cells*. 2017;40(12):897–905.
35. Singh D, Wang SB, Xia T, et al. A biodegradable scaffold enhances differentiation of embryonic stem cells into a thick sheet of retinal cells. *Biomaterials*. 2018;154:158–168.
36. Peng S, Gan G, Rao VS, Adelman RA, Rizzolo LJ. Effects of proinflammatory cytokines on the claudin-19 rich tight junctions of human retinal pigment epithelium. *Invest Ophthalmol Vis Sci*. 2012;53(8):5016–5028.

Investigative Ophthalmology & Visual Science

37. Mao Y, Finnemann SC. Analysis of photoreceptor outer segment phagocytosis by RPE cells in culture. *Methods Mol Biol*. 2013;935:285–295.
38. Livak KJ, Schmittgen TD. Analysis of relative gene expression data using real-time quantitative PCR and the 2(-Delta Delta C(T)) Method. *Methods*. 2001;25(4):402–408.
39. Peng S, Rao VS, Adelman RA, Rizzolo LJ. Claudin-19 and the barrier properties of the human retinal pigment epithelium. *Invest Ophthalmol Vis Sci*. 2011;52(3):1392–1403.
40. Van Itallie CM, Colegio OR, Anderson JM. The cytoplasmic tails of claudins can influence tight junction barrier properties through effects on protein stability. *J Membr Biol*. 2004;199(1):29–38.
41. Rizzolo LJ. Barrier properties of cultured retinal pigment epithelium. *Exp Eye Res*. 2014;126:16–26.
42. Steinberg GR, Kemp BE. AMPK in health and disease. *Physiol Rev*. 2009;89(3):1025–1078.
43. Jansen T, Kvandová M, Daiber A, et al. The AMP-activated protein kinase plays a role in antioxidant defense and regulation of vascular inflammation. *Antioxidants (Basel)*. 2020;9(6):525.
44. Gwinn DM, Shackelford DB, Egan DF, et al. AMPK phosphorylation of raptor mediates a metabolic checkpoint. *Mol Cell*. 2008;30(2):214–226.
45. Dossou AS, Basu A. The emerging roles of mTORC1 in macromanaging autophagy. *Cancers (Basel)*. 2019;11:1422.
46. Lamark T, Svenning S, Johansen T. Regulation of selective autophagy: the p62/SQSTM1 paradigm. *Essays Biochem*. 2017;61(6):609–624.
47. Sherman DJ, Li J. Proteasome inhibitors: harnessing proteostasis to combat disease. *Molecules*. 2020;25(3):671.
48. Zatloukal K, Stumptner C, Fuchsbichler A, et al. p62 Is a common component of cytoplasmic inclusions in protein aggregation diseases. *Am J Pathol*. 2002;160(1):255–263.
49. Sánchez-Martín P, Saito T, Komatsu M. p62/SQSTM1: 'Jack of all trades' in health and cancer. *FEBS J*. 2019;286(1):8–23.
50. Ruttkay-Nedecky B, Nejdl L, Gumulec J, et al. The role of metallothionein in oxidative stress. *Int J Mol Sci*. 2013;14(3):6044–6066.
51. Abul-Hassan K, Walmsley R, Tombran-Tink J, Boulton M. Regulation of tyrosinase expression and activity in cultured human retinal pigment epithelial cells. *Pigment Cell Res*. 2000;13(6):436–441.
52. Julien S, Kociok N, Kreppel F, et al. Tyrosinase biosynthesis and trafficking in adult human retinal pigment epithelial cells. *Graefes Arch Clin Exp Ophthalmol*. 2007;245(10):1495–1505.
53. Valverde P, Manning P, McNeil CJ, Thody AJ. Activation of tyrosinase reduces the cytotoxic effects of the superoxide anion in B16 mouse melanoma cells. *Pigment Cell Res*. 1996;9(2):77–81.
54. Zihni C, Balda MS, Matter K. Signalling at tight junctions during epithelial differentiation and microbial pathogenesis. *J Cell Sci*. 2014;127(pt 16):3401–3413.
55. Bain J, Plater L, Elliott M, et al. The selectivity of protein kinase inhibitors: a further update. *Biochem J*. 2007;408(3):297–315.
56. Ablonczy Z, Dahrouj M, Tang PH, et al. Human retinal pigment epithelium cells as functional models for the RPE in vivo. *Invest Ophthalmol Vis Sci*. 2011;52(12):8614–8620.
57. Luo Y, Zhuo Y, Fukuhara M, Rizzolo LJ. Effects of culture conditions on heterogeneity and the apical junctional complex of the ARPE-19 cell line. *Invest Ophthalmol Vis Sci*. 2006;47(8):3644–3655.
58. Samuel W, Jaworski C, Postnikova OA, et al. Appropriately differentiated ARPE-19 cells regain phenotype and gene expression profiles similar to those of native RPE cells. *Mol Vis*. 2017;23:60–89.
59. Dunn KC, Marmorstein AD, Bonilha VL, Rodriguez-Boulan E, Giordano F, Hjelmeland LM. Use of the ARPE-19 cell line as a model of RPE polarity: basolateral secretion of FGF5. *Invest Ophthalmol Vis Sci*. 1998;39(13):2744–2749.
60. Miyagishima KJ, Wan Q, Corneo B, et al. In pursuit of authenticity: induced pluripotent stem cell-derived retinal pigment epithelium for clinical applications. *Stem Cells Transl Med*. 2016;5(11):1562–1574.
61. Peng S, Gan G, Qiu C, et al. Engineering a blood-retinal barrier with human embryonic stem cell-derived retinal pigment epithelium: transcriptome and functional analysis. *Stem Cells Translational Medicine*. 2013;2(7):534–544.
62. Rizzolo LJ, Peng S, Luo Y, Xiao W. Integration of tight junctions and claudins with the barrier functions of the retinal pigment epithelium. *Prog Retin Eye Res*. 2011;30(5):296–323.
63. Sha Z, Schnell HM, Ruoff K, Goldberg A. Rapid induction of p62 and GABARAPL1 upon proteasome inhibition promotes survival before autophagy activation. *J Cell Biol*. 2018;217(5):1757–1776.
64. Viiri J, Amadio M, Marchesi N, et al. Autophagy activation clears ELAVL1/HuR-mediated accumulation of SQSTM1/p62 during proteasomal inhibition in human retinal pigment epithelial cells. *PLoS One*. 2013;8(7):e69563.

Investigative Ophthalmology & Visual Science